S-Band Dual-Polarization Radar Observations of Winter Storms

PATRICK C. KENNEDY AND STEVEN A. RUTLEDGE

Department of Atmospheric Science, Colorado State University, Fort Collins, Colorado

(Manuscript received 18 May 2010, in final form 28 December 2010)

ABSTRACT

This study is based on analyses of dual-polarization radar observations made by the 11-cm-wavelength Colorado State University–University of Chicago–Illinois State Water Survey (CSU–CHILL) system during four significant winter storms in northeastern Colorado. It was found that values of specific differential phase K_{DP} often reached local maxima of ~0.15°–0.4° km^{-1} in an elevated layer near the −15°C environmental temperature isotherm. The passage of these elevated positive K_{DP} areas is shown to be linked to increased surface precipitation rates. Calculations using a microwave scattering model indicate that populations of highly oblate ice particles with moderate bulk densities and diameters in the ~0.8–1.2-mm range can generate K_{DP} (and differential reflectivity Z_{DR}) values that are consistent with the radar observations. The persistent correlation between the enhanced K_{DP} level and the −15°C temperature regime suggests that rapidly growing dendrites likely played a significant role in the production of the observed K_{DP} patterns. The detection of organized regions of S-band K_{DP} values greater than ~0.1°–0.2° km^{-1} in winter storms may therefore be useful in identifying regions of active dendritic particle growth, as a precursor to aggregate snowfall.

1. Introduction

The Colorado State University–University of Chicago–Illinois State Water Survey (CSU–CHILL) radar has collected data from a number of winter storms that affected northeastern Colorado in recent years. These have primarily been target-of-opportunity operations in which various dual-polarization data-collection procedures and antenna scanning procedures have been tested. One pattern that has been frequently observed in the dual-polarization data fields is the development of mesoscale regions of modest values of S-band specific propagation phase (K_{DP}) (~0.2°–0.6° km^{-1}) that frequently occur near the −15°C temperature level. These K_{DP} areas are most evident during the more intense periods of the observed winter storms. Observations of weak positive K_{DP} areas located above the surface in winter storms have been previously reported by Trapp et al. (2001). Ryzhkov et al. (1998) have documented the generation of detectable S-band K_{DP} values from horizontally oriented ice particles at an altitude of ~6 km in the trailing precipitation region of a squall line. The preferential growth of dendritic ice crystals at temperatures around −15°C has also been found to contribute to the development of positive differential reflectivity (Z_{DR}) layers within cold-season precipitation systems (Andric et al. 2010). This paper is focused on the structure of the K_{DP} fields observed in four intense winter-storm events. Observations of organized positive K_{DP} patterns near the −15°C environmental temperature level appear to identify regions of particularly active dendritic particle growth. A numerical model of microwave scattering is used to gain additional insights into the dual-polarization data values expected from various populations of crystalline and low-density aggregate-type ice particles. Basic calculations of ice crystal growth via vapor deposition are also used to support the probable existence of K_{DP}-producing ice crystals in these observed winter storms.

2. Overview of the polarimetric data

The radar data were collected by the 11-cm-wavelength CSU–CHILL National Radar Facility located near Greeley, Colorado, at an elevation of 1432 m MSL. The antenna pattern has a 3-dB beamwidth of ~1.0°, and its horizontal (H) and vertical (V) polarization ports are driven by identical Klystron-based FPS-18 transmitters. The data presented here were collected with the transmit polarization alternating between H and V on a pulse-to-pulse basis. Scan rates were typically 6°–10° s^{-1} during plan

Corresponding author address: Patrick C. Kennedy, Dept. of Atmospheric Science, Colorado State University, Fort Collins, CO 80523.
E-mail: pat@chill.colostate.edu

DOI: 10.1175/2010JAMC2558.1

position indicator (PPI) scans and ~$1^{\circ}\,s^{-1}$ during RHI scans. (Brunkow et al. 2000. At the time of writing, additional information on the radar could be found at the CSU–CHILL Internet site (http://www.chill.colostate.edu).

The difference in the relative phase of the copolar H and V received signals is the basis of the measurement of propagation differential phase ϕ_{dp}. Positive differential propagation phase shifts (increasing phase lag of the H return signal with respect to the V signal) arise from the collective effects of oblate scatterers along the radar beam path. Positive ϕ_{dp} shifts will be generated when the radar pulses propagate through many distinctly oblate, large, high-permittivity scatterers. Specific propagation differential phase K_{DP} is the range derivative of ϕ_{dp}. Portions of the beampath in which a significant H signal phase lag is accumulating will be characterized by relatively large positive K_{DP} values. In the case of ice particles, positive K_{DP} signatures are most effectively produced by appreciable concentrations of relatively pristine platelike ice crystals, grown by vapor deposition. Under the simplifying assumptions that the bulk density and axis ratio of the plates are invariant with respect to diameter, the theoretical K_{DP} generated by platelike ice crystals is approximated by [Bringi and Chandrasekar 2001, their Eq. (7.101)]

$$K_{DP} = 10^{-3} \times (180^{\circ}/\lambda) C\rho_p \times \mathrm{IWC} \times (1 - r), \quad (1)$$

where K_{DP} is specific propagation differential phase in degrees per kilometer, λ is the radar wavelength in meters, C is a constant that is approximately equal to 1.6 $(\mathrm{g\ cm^{-3}})^{-2}$ for Rayleigh scattering conditions, ρ_p is the plate particle bulk density in grams per centimeter cubed, IWC is the ice water content of the platelike ice crystals in grams per meter cubed, and r is the particle axis ratio (vertical/horizontal length dimension ratio). The K_{DP} magnitudes will increase in echo areas where platelike (i.e., small axis ratio) ice particles with relatively high bulk densities exist in numbers that generate appreciable ice water contents. The estimation of K_{DP} generally involves the application of various filtering and curve-fitting procedures to the directly observed range profile of ϕ_{dp} (Hubbert and Bringi 1995). In this paper, K_{DP} was calculated following the methods of Wang and Chandrasekar (2009).

Differential reflectivity Z_{DR} is the ratio of the copolar Z_{hh} and Z_{vv} reflectivities expressed on a logrithmetic scale:

$$Z_{DR}(\mathrm{dB}) = 10\log_{10}(Z_{hh}/Z_{vv}). \quad (2)$$

The diameter of oblate particles is larger in the horizontal plane than in the vertical plane, and therefore the Z_{DR} observed from such particles is positive, typically on the order of several decibels. Differential reflectivity is an expression of the reflectivity-weighted mean axis ratio of the particle size distribution (PSD; Jameson 1983). Therefore, because reflectivity is a strong function of particle diameter D, the observed Z_{DR} may not be representative of the shape characteristics of the lower-reflectivity (typically smaller) members of the particle population. In the case of snow, the presence of sufficient quasi-spherical, large aggregates can effectively obscure the distinctly positive Z_{DR} values that are characteristic of highly oblate but small-diameter ice crystals. It is important to note that K_{DP}'s mass-weighted (D^3) sensitivity to particle axis ratio (as opposed to Z_{DR}'s D^6 weighting) minimizes the "masking" effect of the quasi-spherical aggregates. The detection of positive K_{DP} areas within ice cloud echoes signifies the presence of an appreciable population of relatively dense, low-axis ratio plate/dendritic-type particles within the overall assemblage of hydrometeors.

3. Case studies

a. 28 October 2009

On 28 October 2009, deep cyclonic upslope flow produced widespread heavy snow in the CSU–CHILL radar coverage area (Dunn 1988). One period of relatively high snowfall rates took place within a few hours of a surface cold-frontal passage that occurred around 0000 UTC. Figure 1a shows the 2.7°-elevation PPI reflectivity data at 0441 UTC. To aid contour plotting, the data have been interpolated to a 1 km × 1 km Cartesian grid on the PPI scan surface using the National Center for Atmospheric Research (NCAR) sorted position radar interpolation program (SPRINT; Mohr and Vaughan 1979; Miller et al. 1986). The grid origin is at the CSU–CHILL radar (marked as CHL). The three range rings have been added to indicate the distances at which the beam height reached the −10°, −15°, and −20°C temperature levels according to the 0000 UTC Denver (Colorado) radiosonde data. (In the subsequent 1200 UTC sounding, cold-air advection had lowered the heights of these isotherms by an average of 450 m. This would reduce the range to the reference temperature levels by ~10 km.) The Marshall field site operated by NCAR is marked at $X = -50$, $Y = -55$ km. After 0200 UTC, the Marshall observations included moderate to heavy snow and surface winds from directions between ~20° and 320°. During the 0000–0500 UTC period, the mean motion of the echoes observed on the 2.7° PPI scans was generally from the south at 6 m s^{-1}. In the 0441 UTC PPI scan shown in Fig. 1a, the major axis of one of these translating echo masses was located ~30–40 km northeast (i.e., approximately upstream) of Marshall. Figure 1b shows the

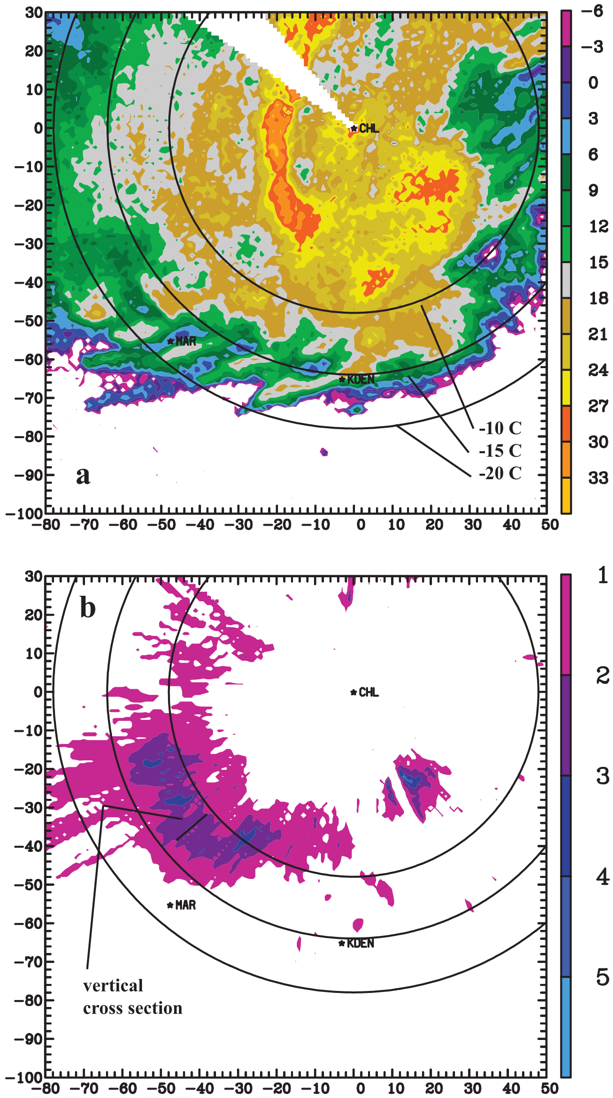

FIG. 1. The (a) 2.7° reflectivity PPI (isotherms are indicated by the thick black lines as labeled) and (b) 2.7° PPI of $K_{DP} \times 10$ (the location of the vertical cross section shown in Fig. 2 is indicated) at 0441 UTC 28 Oct 2009.

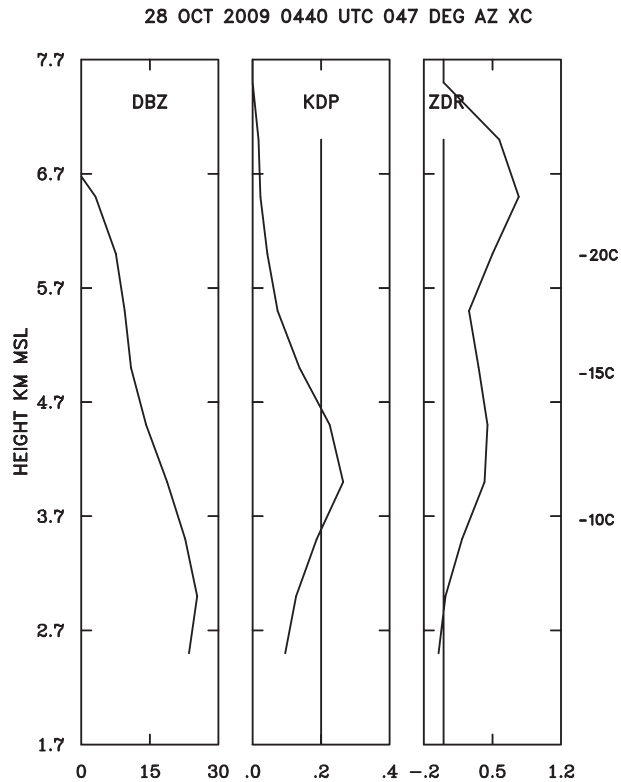

FIG. 2. Vertical profiles of reflectivity, K_{DP}, and Z_{DR} at 0441 UTC 28 Oct 2009. Data are taken from gridded values in the rotated cross section shown in Fig. 1b. Temperatures along the right edge of the plot are from the Denver 0000 UTC 28 Oct 2009 sounding.

corresponding K_{DP} field in the 2.7° PPI sweep. (The K_{DP} values have been scaled up by a factor of 10; a color scale value of 2 indicates a K_{DP} of 0.2° km^{-1}). An area of K_{DP} values exceeding 0.1° km^{-1} was associated with the echo mass located to the northeast of Marshall. This positive K_{DP} area was primarily found at higher altitudes (i.e., greater ranges) than the maximum reflectivities seen in Fig. 1a. The highest K_{DP} magnitudes (0.2°–0.3° km^{-1}) were generally observed between the −10° and −15°C temperature levels.

The vertical profiles of the radar measurements in a vertical section through the echo region located to the northeast of Marshall at 0441 UTC are shown in Fig. 2. The data included in the profiles were obtained by interpolating the measurements obtained in a sequence of PPI sweeps to the 8-km-long vertical cross section shown in Fig. 1b. As will be shown in the subsequent particle trajectory discussion, this cross section was located in the probable source region for snow that was falling at Marshall. The heights of the selected environmental temperature values shown along the right edge of the plot were obtained from the 0000 UTC Denver radiosonde data. Reflectivity values showed a general increase toward the surface, presumably owing to the development of an increasing number of large aggregates. As suggested by the PPI plots, the largest K_{DP} values were found in the vicinity of the −15°C isotherm, above the heights associated with largest reflectivities. Positive differential reflectivity values of a few tenths of a decibel were present throughout most of the profile. The largest positive values were found at heights above ~6.5 km in the profile, with a minor positive Z_{DR} peak located at and slightly above the maximum K_{DP} height. Below this level, Z_{DR} decreased to essentially 0 dB at the lowest heights.

The trends in the vertical profiles are in agreement with the signatures of snow particle aggregation reported by

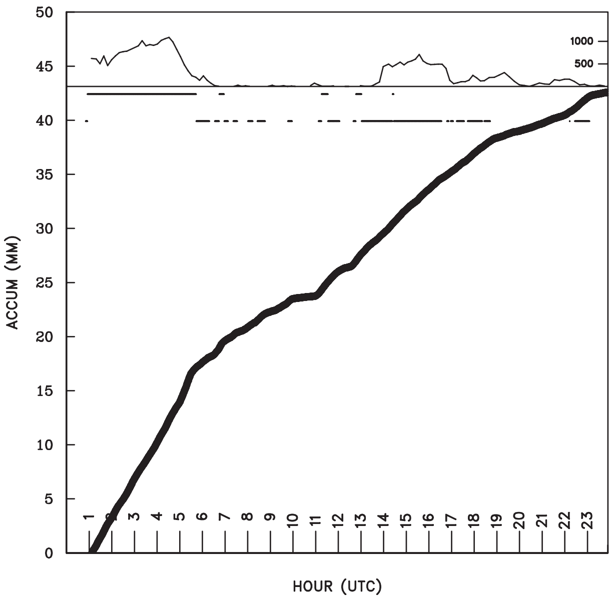

FIG. 3. Time series of observations of the 28 Oct 2009 snowstorm at the Marshall field site operated by NCAR. Upper thin trace is count of the number of grid points with K_{DP} values of 0.1° km^{-1} on the 2.7° PPI sweep. These counts were collected in a 60 km × 60 km box centered on Marshall. Lower thick trace is liquid precipitation accumulation observed at Marshall. Broken horizontal line segments plotted just below the gridpoint counts depict times when the surface precipitation rate exceeded 1.5 mm h^{-1} (lower trace) and 2.5 mm h^{-1} (upper trace).

Ryzhkov and Zrnic (1998): near the echo top, low concentrations of relatively pristine, quasi-horizontally oriented crystals probably existed. In qualitative terms, this particle population would be expected to produce low reflectivities, distinctly positive Z_{DR} values, and essentially no K_{DP}. In the lowest portions of the height profile, large, irregularly shaped, low-density aggregates would have developed through aggregation of the more pristine, planar ice crystal forms. The general shift from a crystal-dominated to an aggregate-dominated particle population at the lower height levels would be expected to enhance reflectivity while correspondingly reducing Z_{DR} and K_{DP}. We will return to this point using scattering calculations later.

A time history of the precipitation accumulation at Marshall and the number of nearby grid points with K_{DP} magnitudes of 0.1° km^{-1} or more is shown in Fig. 3. The precipitation accumulation was obtained from a gauge designed for the observation of winter-season precipitation (a Geonor, Inc., Model T-200 vibrating-wire tranducer gauge equipped with a heated inlet and installed inside a double Alter wind screen; S. Landolt 2010, personal communication). The gridpoint counts shown in the upper portion of the figure were obtained by examining a 60 km × 60 km area centered on Marshall, on the 2.7° PPI surface. The number of Cartesian grid points within this domain that had K_{DP} magnitudes greater than or equal to 0.1° km^{-1} was tabulated for each PPI sweep; this elevation angle was selected because it intersected the −15°C altitude within ~30 km of Marshall. The precipitation history indicates that two higher-intensity precipitation periods took place: 0100–0600 and 1300–1800 UTC, with lighter snowfall rates being observed at Marshall during the intervening overnight hours. A symbolic representation of precipitation rate calculated from the gauge trace is shown by the two broken horizontal lines plotted in the upper portion of the figure. The lower line appears at times when the liquid equivalent precipitation rate exceeded 1.5 mm h^{-1}; the upper line is marked when the rate exceeded 2.5 mm h^{-1}. The crossings of these precipitation-rate thresholds highlight the two-pulse nature of the storm's precipitation production. The K_{DP} trace at the top of the figure contained two corresponding time periods during which significant numbers of grid points with detectable K_{DP} values were present aloft within ~30 km of the Marshall site. During the intervening 0700–1200 UTC light-snowfall period, little or no measurable S-band K_{DP} was detected in the vicinity of Marshall.

Particle trajectory calculations were done to examine further the connection between a time of high snowfall rates at the surface and the existence of positive K_{DP} areas aloft. These calculations use three-dimensional air motion fields derived from multiple Doppler wind field syntheses to advect the particles. Parameterization equations are used to assign particle terminal velocity values are each time step (Knight and Knupp 1986). For this application, input radial velocity data from the Denver (KFTG) Weather Surveillance Radar-1988 Doppler (WSR-88D) were combined with those from CSU–CHILL to develop wind field syntheses at two times at which the radars began volume scans within 1 min of each other (0340 and 0431 UTC). The long (74 km) baseline between these radars limits the spatial resolution available in the analysis, but the resolution is adequate for the horizontal wind field features typically observed in winter storms. Data processing was done using NCAR's SPRINT and Custom Editing and Display of Reduced Information in Cartesian Space (CEDRIC; Miller et al. 1986) software. Cartesian gridpoint spacings were 1 km in the horizontal plane and 0.5 km in the vertical direction. Vertical air motions were calculated by applying a variational scheme to redistribute the errors that were initially observed at the integration boundaries. These calculated vertical air velocities typically have standard error magnitudes of 1–3 m s^{-1} (Rasmussen et al. 1993), which are likely greater than the mesoscale vertical velocities present in winter storm systems. Thus, the results of the trajectory

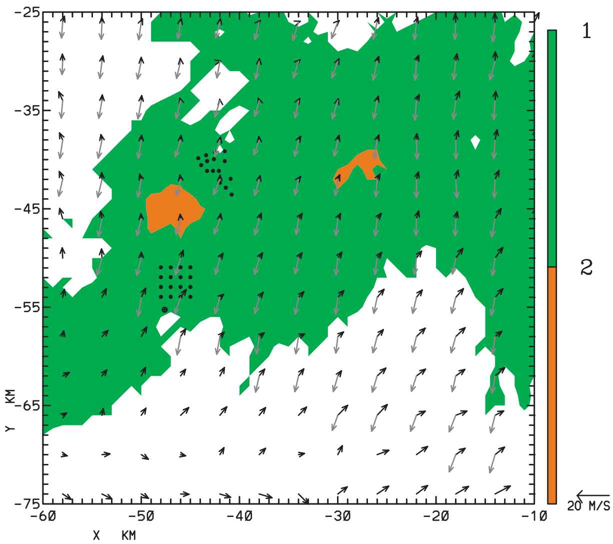

FIG. 4. Particle-trajectory results for the 28 Oct 2009 case. Trajectories were initiated at 2.8 km MSL (the lowest dual-Doppler wind analysis height) from the square set of grid points located just north of Marshall [larger dot at (-50, -55)]. Particle locations were calculated backward in time until they reached the height of the -15°C level; these endpoints are marked by the dot cluster near (-40, -40). Black wind vectors are the time-averaged horizontal winds at 5.1 km MSL during the 50-min trajectory-calculation period. Gray arrows are the similarly time-averaged horizontal winds at 2.8 km MSL. Color fill is the time-averaged K_{DP} field at 5.1 km MSL (° km^{-1} × 10).

calculations are at best only a very general depiction of the actual snow particle paths.

The trajectory results for the 0340–0431 UTC time period are shown in Fig. 4. The color-coded wind vectors depict the average Earth-relative horizontal flow near 5 km MSL (within the positive K_{dp} region) and at the lowest analysis height (2.8 km MSL). The contours show the time-averaged K_{dp} values in the 4.8–5.3-km height layer. Particles were initiated from the rectangular region just north of Marshall at 2.8 km MSL at 0431 UTC; backward trajectories were then calculated until they reached the 5 km MSL altitude. (Commensurate with a typical snow particle fall velocity of ~1 m s^{-1} and a height change of ~2.2 km, the durations of these trajectories were ~37–46 min.) The calculations indicate that the particles reaching the Marshall area in the form of heavy snow observed at 0431 UTC were likely associated with the positive K_{dp} region located ~30 km northeast of Marshall near the -15°C temperature level between 0340 and 0431 UTC. Because of the inherent uncertainties in the vertical air velocities and in the snow particle terminal velocities, it is unwise to place too much credence in the specifics of these trajectory results. Nevertheless, the mostly uniform horizontal flow fields in combination with average snow particle fall speeds of ~1 m s^{-1} support the general linkage between the positive K_{dp} region observed aloft to the northeast of Marshall between 0340 and 0431 UTC and existence of enhanced snowfall rates at the surface.

b. 20 December 2006

CSU–CHILL radar data were collected during a major winter storm that began to impact the area on 20 December 2006. Like the previous event, the synoptic environment over northeastern Colorado supported the development of strong easterly flow that extended upward to midtropospheric heights. This resulted in a combination of heavy snowfall and high surface winds during much of the daytime hours of 20 December. As the day progressed, these winter-storm conditions increasingly had an impact on operations at Denver International Airport (KDEN). Flight operations were ultimately suspended at ~2137 UTC.

Figure 5a shows the reflectivity pattern observed in a 3.5°-elevation-angle PPI scan at 1505 UTC, when reports of heavy snow began to appear in the KDEN surface observations. KDEN is located near $X = -3$, $Y = -65$ km. As in Fig. 1a, the three range rings indicate where the beam height reached the -10°, -15°, and -20°C temperature levels according to the 1200 UTC Denver radiosonde data. The echo coverage on the 3.5° PPI scan had been steadily expanding westward and intensifying during the preceding hour. The associated K_{DP} plot showed a large region containing >0.2° km^{-1} values in the CHILL's southeastern azimuth quadrant (Fig. 5b). Within this region, the maximum K_{DP} values remained in fairly close proximity to the -15°C altitude.

RHI scans along the ~157° azimuth provide a more detailed view of the vertical structure of the echo mass located northeast (upstream in terms of the low-level winds) from KDEN. At 1502 the maximum reflectivities (~24–28 dBZ) were found near the surface (Fig. 6a). Positive K_{DP} values maximized in a layer centered near 3 km AGL (Fig. 6b). The Z_{DR} field also contained a well-defined relative maximum at midlevel heights (~3 km AGL) within the general echo depth (Fig. 6c). Like the enhanced K_{DP} layer, the level of maximum positive Z_{DR} values was found above the surfaced-based high-reflectivity region.

Figure 7 shows a more detailed view of the data values extracted from the 20–28-km range interval in the RHI scan shown in Fig. 6. The largest positive K_{DP} values were found near the 4.7 km AGL level where the sounding temperature was very near to -15°C. The Z_{DR} values maximized several hundred meters higher at temperatures that were closer to -20°C. The most intense reflectivities were found in the lowest 1 km of the profile, well below the heights of both the K_{DP} and Z_{DR} maxima.

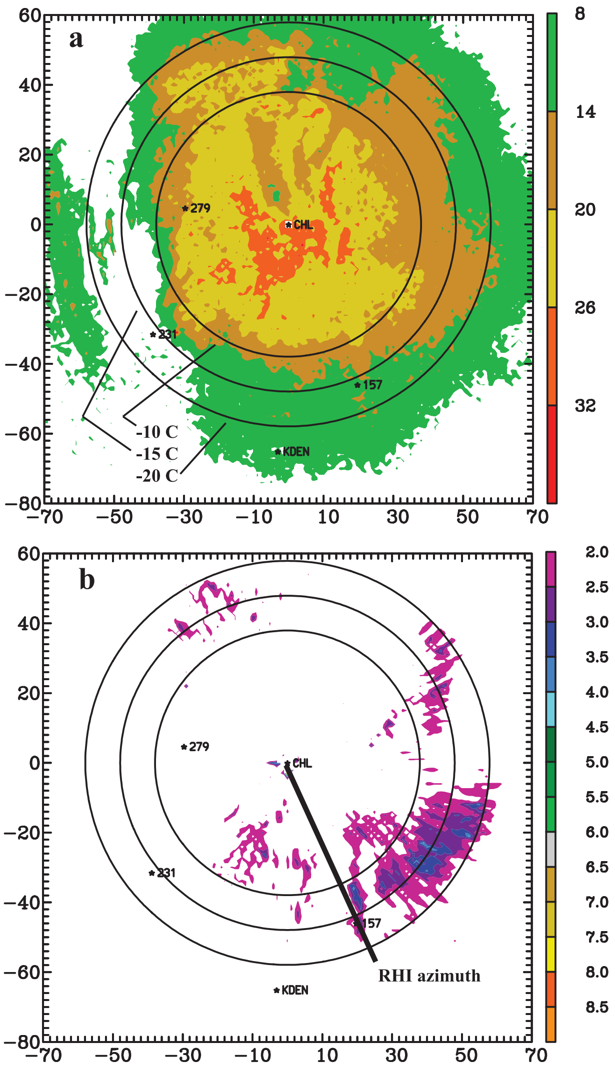

FIG. 5. The (a) 3.5° reflectivity PPI (isotherms are as in Fig. 1a) and (b) 3.5° PPI of $K_{DP} \times 10$ (thick line shows the location of the RHI scan in Fig. 6) at 1505 UTC 20 Dec 2006.

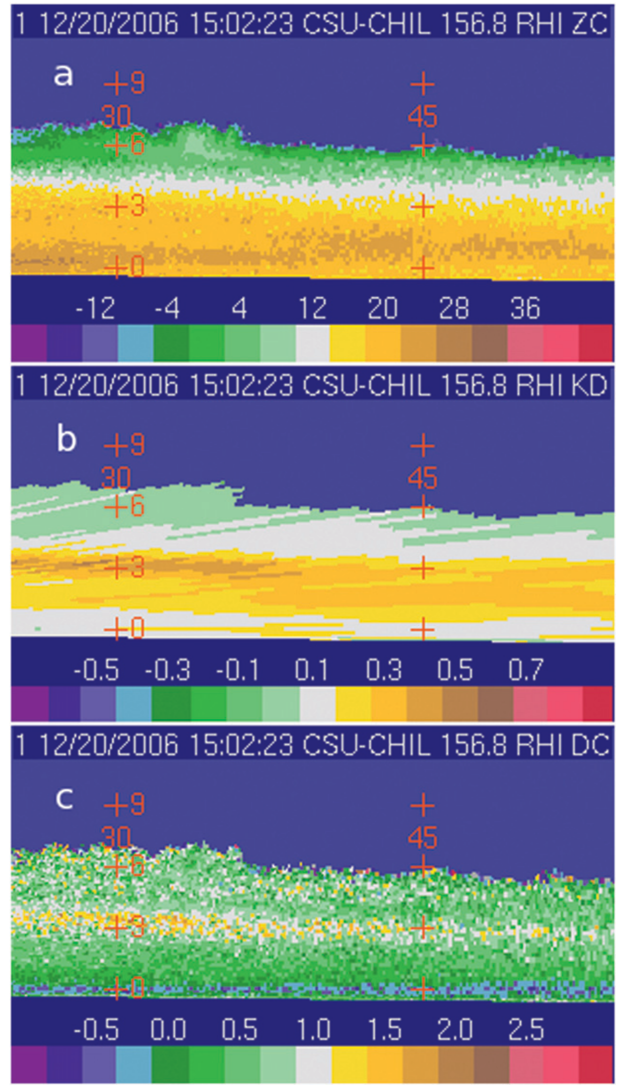

FIG. 6. The 157° RHI at 1502 UTC 20 Dec 2006: (a) reflectivity (dBZ), (b) K_{DP} (° km^{-1}), and (c) Z_{DR} (dB).

The vertical structure of the data fields contained in these RHI scans is very similar to the profiles that were shown for the 28 October 2009 case.

Following the plotting conventions of Fig. 3, Fig. 8 combines time histories of surface precipitation observations and the number of grid points with K_{DP} values exceeding 0.1° km, in a 60 km × 60 km domain centered on KDEN. The precipitation data were collected by a Geonor gauge operated by NCAR at KDEN. To reduce the effects of wind, this gauge was installed inside a double Alter-type wind screen. Because the average surface wind speeds frequently exceeded 15 m s^{-1} at KDEN, however, some of the snow probably failed to enter the gauge (S. Landolt 2010, personal communication). Precipitation accumulation began near 1400 UTC, with rates often exceeding 2.5 mm h^{-1} (water equivalent) between 1500 and 1700 UTC. As in the previous case, the time history of the count of grid points exceeding 0.1° km^{-1} in the 3.5° PPI scan in the vicinity of KDEN showed a general correlation with the observations of higher snowfall rates at the surface.

c. *16–20 March 2003*

During the period of 16–20 March 2003, snow accumulations of historic proportions took place over the western half of the CSU–CHILL radar's standard 150-km operating range (Poulos et al. 2003). One 12-h period of heavy snow (hourly liquid equivalent precipitation amounts of ~3.2 mm or more measured in Fort Collins, Colorado) began during the afternoon hours of 18 March 2003. Figure 9a shows the reflectivity field on the 4.2° PPI

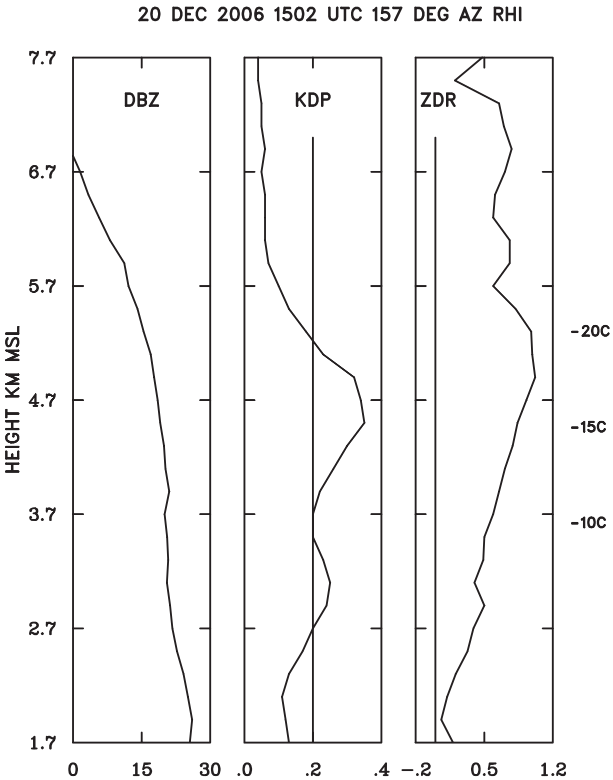

FIG. 7. Vertical data profiles extracted from the 20–28-km range interval in the RHI scan shown in Fig. 5. Temperatures along the right edge of the plot are from the Denver 1200 UTC 20 Dec 2006 sounding.

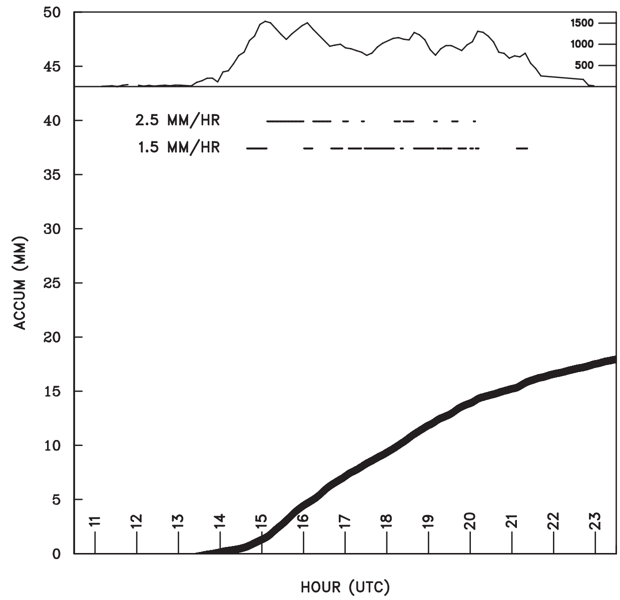

FIG. 8. As in Fig. 3, but for the NCAR mesonet gauge located at the Denver International Airport.

surface at 2004 UTC. Range rings have again been added where the beam height reached the −10, −15, and −20°C heights in accord with the 12-h global Aviation Model (AVN) forecast valid at 1800 UTC. (Because of the unfavorable launch conditions, no Denver soundings were available on 18 March.) At 2004 UTC, an area of reflectivities with values of 20–30 dBZ had passed over the CSU–CHILL radar site and had moved west–northwestward toward the Fort Collins area where a recording precipitation gauge operated by the state climate survey office (location marked by KFCL) was starting to measure an enhanced snowfall rate. An area of positive K_{DP} values that maximized near the −15°C temperature level was present just north of KFCL as the higher precipitation rates were beginning to occur at 2004 UTC (Fig. 9b).

Figure 10 shows data from an RHI scan that was done at 1943 UTC on an azimuth of 287°. This RHI intersected the echo area that would reach the Fort Collins area and generate the increased snowfall rates starting near 2004 UTC. This RHI contained features similar to those seen in the 20 December 2006 case (Fig. 6): well-defined layers of locally enhanced positive K_{DP} and Z_{DR} values were detected at midecho height in association with reflectivity levels of ~20 dBZ; steadily greater reflectivities were present toward the surface.

Vertical profiles of selected radar measurements from the 16–24-km range increment of the 1943 UTC RHI scan are shown in Fig. 11. The K_{DP} values reached a peak of ~0.3° km^{-1} near the 4.2 km MSL level; as in the earlier cases this was near to the height of the −15°C environmental isotherm. The positive Z_{DR} layer was centered somewhat higher near 4.7 km MSL, consistent with the previous cases.

d. 23–24 March 2010

Rain changed over to heavy snow across the greater Denver area during the final (UTC) hours of 23 March 2010. At 0045 UTC on 24 March, the snowfall conditions at KDEN began to cause serious disruptions to the deicing of departing aircraft. The intense precipitation rates began to decrease in the Denver area after ~0400 UTC. Data collected in a 2.75° PPI scan at 0026 UTC are shown in Fig. 12. Reflectivity levels in excess of 25 dBZ were common over much of the area at this elevation angle (Fig. 12a). Enhanced K_{DP} values were also widespread, with large areas reaching magnitudes of 0.3–0.4° km^{-1} (Fig. 12b).

Observations collected in a 220.8° azimuth RHI sweep done at 0035 UTC are shown in Fig. 13. As in the previous events, reflectivity generally increased toward the surface, especially in the lowest ~3 km (Fig. 13a). The largest positive K_{DP} values (Fig. 13b) were present in an elevated layer centered near ~3 km AGL (4.2 km MSL; −12.5°C in the Denver sounding data.) The Z_{DR} field also contained

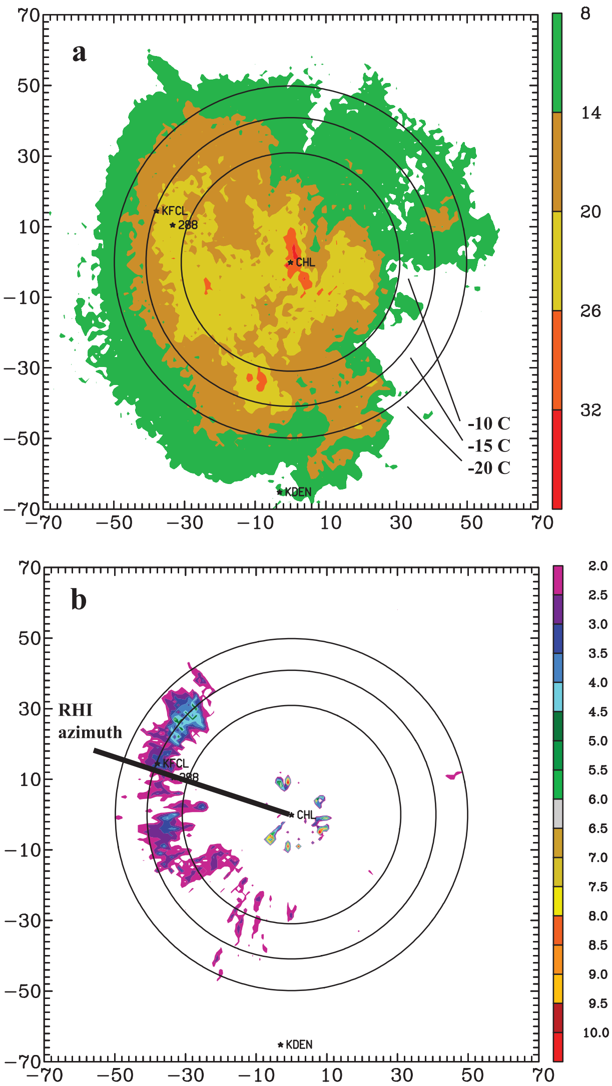

FIG. 9. The 18 Mar 2003 case: (a) 4.23° PPI reflectivity (dBZ; isotherms are from the 12-h AVN model forecast valid at 1800 UTC) at 2002 UTC and (b) 4.23° PPI of $K_{DP} \times 10$ at 2004 UTC.

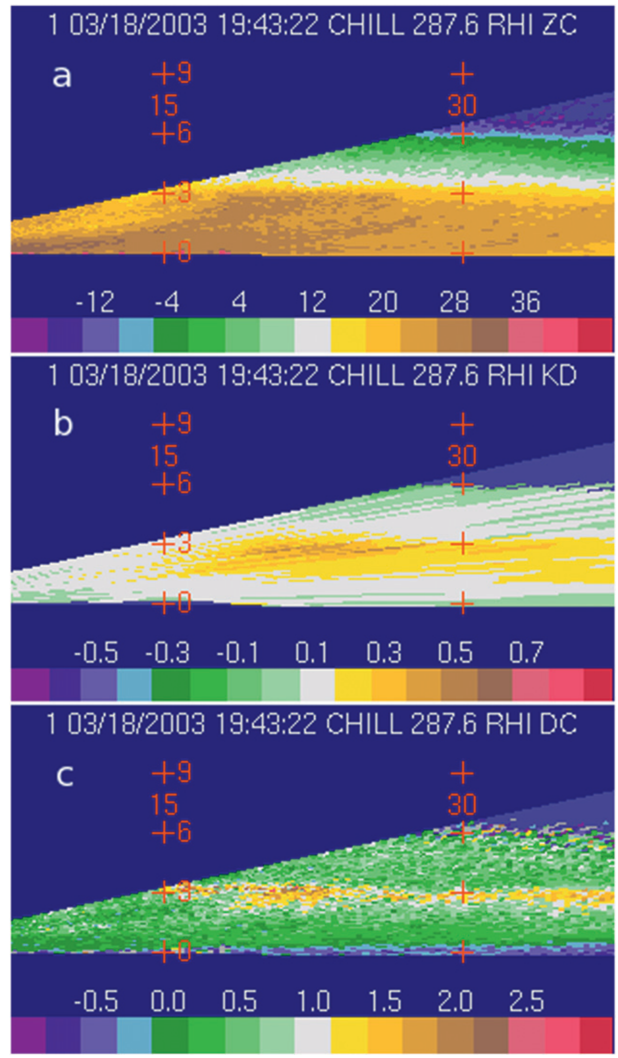

FIG. 10. The 287.6° RHI at 1943 UTC 18 Mar 2003: (a) reflectivity (dBZ), (b) K_{DP} (° km^{-1}), and (c) Z_{DR} (dB).

a slight relative maximum near the 3-km height (Fig. 13c). An expanded view of these patterns is shown in the vertical profiles contained in Fig. 14. The K_{DP} enhancement was located in a fairly thick layer that reached a maximum at 4.3 km MSL; this was above the heights that contained the most-intense reflectivities (Figs. 13a and 13b). The Z_{DR} profile contained a double-maxima structure with peaks at 4.9 and 4.1 km MSL.

As was done for the 28 October 2009 case, time histories of selected parameters pertaining to the Marshall field site are shown in Fig. 15. The Marshall observers reported a change from mixed rain and snow to mostly snow at 2100 UTC; within the next 15 min the snow became heavy. As shown by the rate category codes in the upper portion of Fig. 15, liquid equivalent precipitation rates consistently exceeded 2.5 mm h^{-1} between 2200 and 0300 UTC. During this same period, the tally of grid points with K_{DP} values at or above 0.1° km^{-1} on the 2.75° PPI surface within ~60 km of Marshall frequently exceeded 1000.

Using the methods described in the October 2009 case, particle trajectory calculations were done for the 0010–0050 UTC period on 24 March 2010; the results are shown in Fig. 16. In the height layer with temperatures of ~−15°C, winds were generally from the southeast. Positive K_{DP} magnitudes of several tenths of a degree per kilometer were extensive at this height. At the lowest analysis level (2.5 km MSL), the dual-Doppler retrieval found strong northeasterly flow. The backward trajectory results indicated that snow particles in the heavy precipitation observed at Marshall around 0050 UTC were probably located in

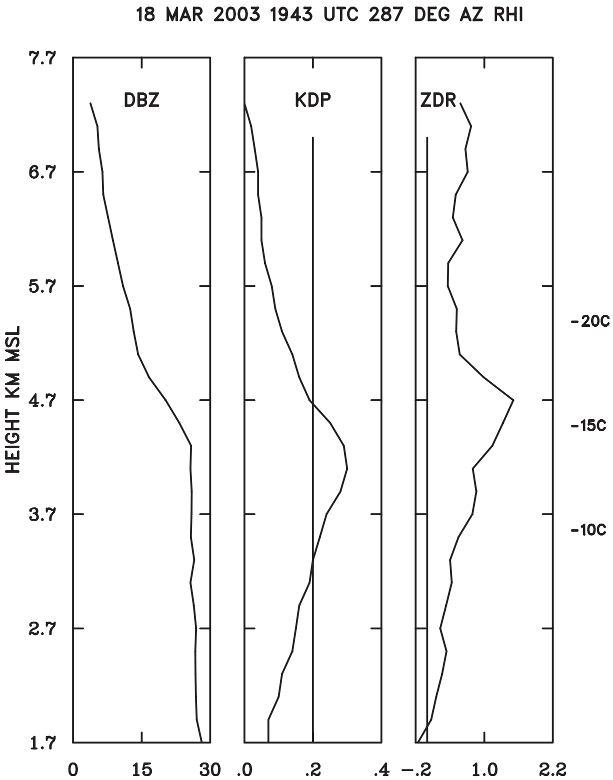

FIG. 11. Vertical data profiles extracted from the 16–24 range interval of the RHI scan shown in Fig. 9.

the positive K_{DP} layer near the $-15°C$ level approximately 45 min earlier.

The areal extent and magnitude of the positive K_{DP} field observed on the 2.75° PPI surface expanded steadily after ~2330 UTC. The patterns shown in Fig. 12 are indicative of the maximum K_{DP} developmental stage in the Denver area; K_{DP} enhancement was significantly reduced after 0200 UTC. To examine the relationship between low-level upslope flow and the observed K_{DP} life cycle, averages of the dual-Doppler synthesized horizontal wind fields were developed for a sequence of five times at which the CSU–CHILL and KFTG radars started volume scans within ±2.5 min of each other. (The domain over which these wind field averages were computed is shown in Fig. 12.) The resultant wind speeds and directions are plotted in time–height format in Fig. 17. Within this analysis domain, terrain heights begin to increase rapidly just west of a line connecting Marshall and Golden, Colorado (see Fig. 12). Maximum terrain heights reach 4 km MSL at points near the western edge of the grid. Between 2339 and 0051 UTC, the upslope (from the northeast quadrant) flow strengthened appreciably below 3.5 km MSL. By 0221, the wind directions had backed to a more northerly direction, reducing the upslope flow component. The development of a relatively large, well-organized positive

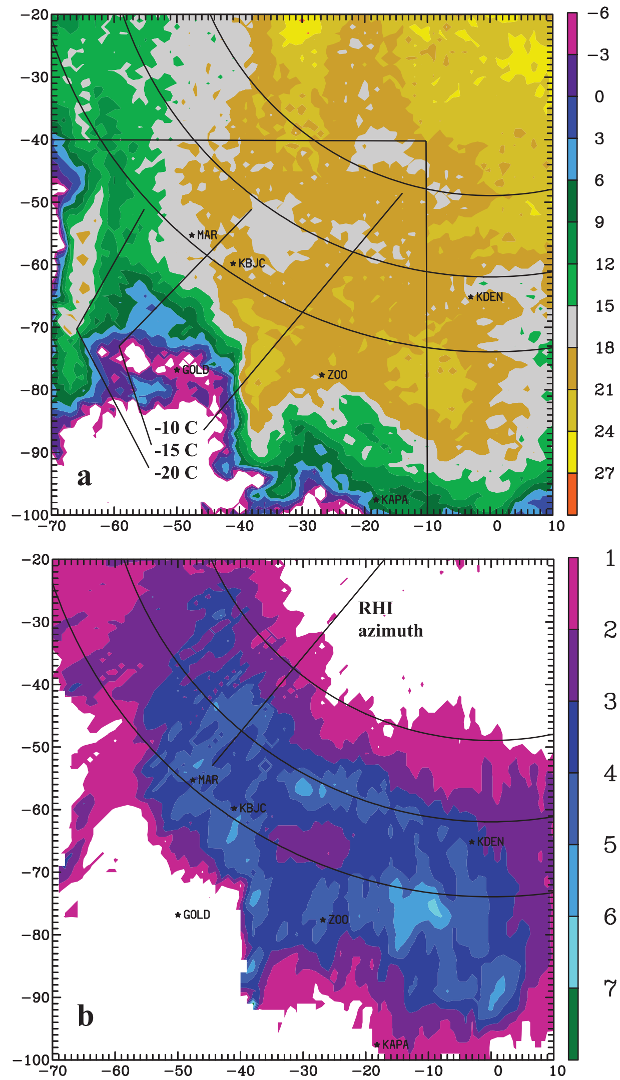

FIG. 12. (a) CSU–CHILL 2.75° PPI data at 0026 UTC 24 Mar 2010 for reflectivity (dBZ). Rings mark where the beam height is equal to selected environmental temperatures according to the 0000 UTC Denver radiosonde observations. The square region marked in the southwestern portion of the plot shows the domain over which dual-Doppler U and V wind components were averaged (see text and Fig. 14). Selected base-map locations are (from top to bottom) Marshall (MAR), Rocky Mountain Metropolitan Airport (KBJC), Denver International Airport (KDEN), Golden (GOLD), Denver Zoo surface weather observation site (ZOO), and Centennial Airport (KAPA). (b) As in (a) but data are K_{DP} (° km^{-1} × 10).

K_{DP} area aloft coincided with the period of enhanced low-level upslope flow. We suggest that the strengthening upslope flow increased the upward vertical motions at the $-15°C$ level, promoting water-saturated conditions and rapid dendritic particle growth, and caused the enhanced K_{DP} signature. Later, we will return to this point from the perspective of a simple particle growth model via deposition.

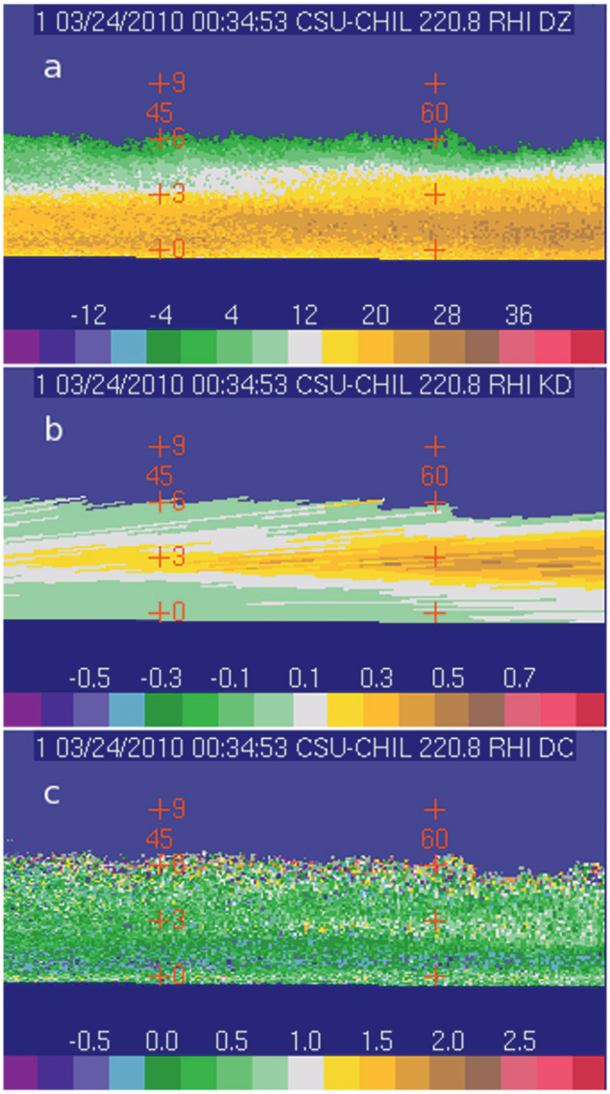

FIG. 13. RHI data from azimuth 220.8° at 0035 UTC 24 Mar 2010: (a) reflectivity (dBZ), (b) K_{DP} (° km^{-1}), and (c) Z_{DR} (dB).

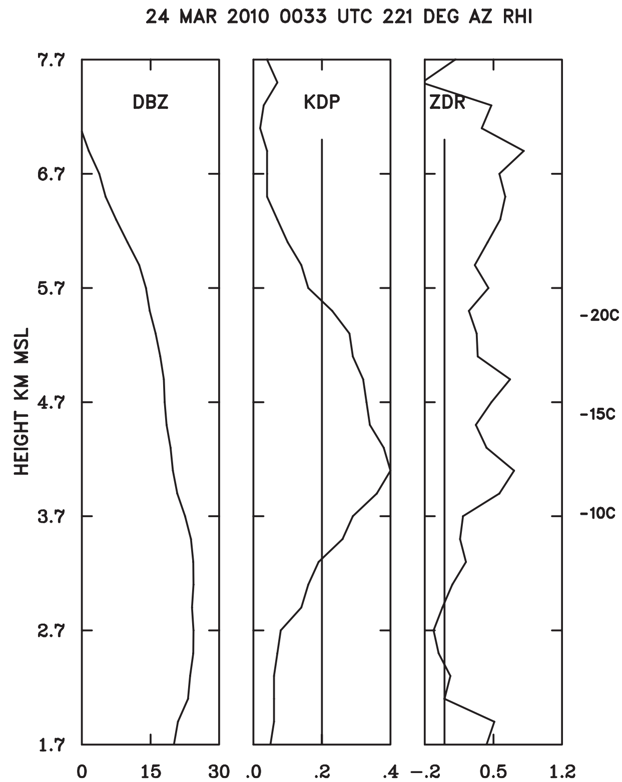

FIG. 14. Vertical profiles based on the data in the 56–64-km range interval of the RHI shown in Fig. 13. Environmental temperatures shown along the right edge of the plot are from the 0000 UTC Denver radiosonde data.

Taken together, all four of the winter-storm cases contained evidence of a common vertical structure in echo areas that were associated with relatively high surface snowfall rates: positive (>0.1° km^{-1}) K_{DP} values were detected in the vicinity of the −15°C environmental temperature level, which was typically located in the middle levels of the entire echo system. An associated layer of positive Z_{DR} was generally found a few hundred meters above the height of maximum K_{DP}. This localized positive Z_{DR} enhancement may have been due to the presence of supercooled droplets (Hogan et al. 2002; Moisseev et al. 2009) that promoted the growth of dendritic crystals. Between the positive K_{DP} layer and the surface, the dual-polarization signatures tended to diminish while reflectivity values increased to their maximum intensities. These polarimetric patterns were detectable for multihour periods during the winter-storm events; they typically were best defined when significant surface snowfall rates existed. To a first approximation, the vertical stratification of the radar observations suggests that a significant concentration of quasi-horizontally oriented ice particles was present near the −15°C temperature level. The subsequent collection of these particles into larger, lower-bulk-density, irregularly shaped aggregates caused the K_{DP} and Z_{DR} magnitudes to decrease at lower heights.

4. Microwave scattering calculations

To investigate the dual-polarization microwave scattering characteristics of specified populations of frozen hydrometeors that may have lead to the polarimetric signatures described above, we employed the transmission matrix (T matrix) method (Waterman 1971; Barber and Yeh (1975). Although this numerical method can have convergence problems for highly oblate particle shapes (Bringi and Chandrasekar 2001, their appendix 3), satisfactory results were obtained for ice particles with relative permittivity values significantly below that of water.

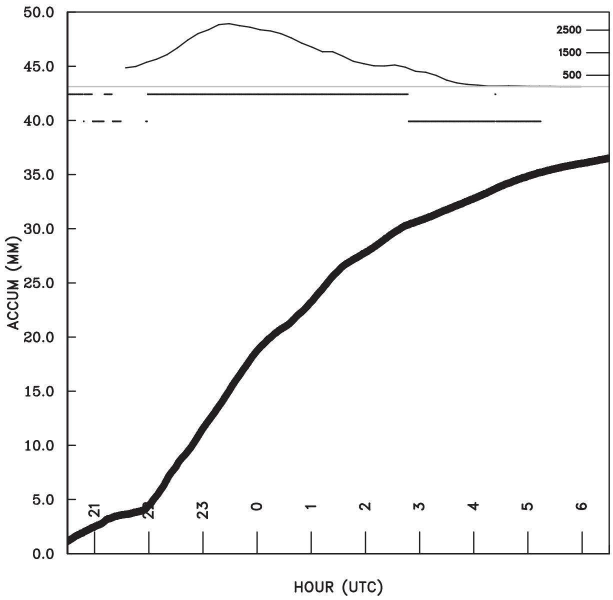

FIG. 15. As in Fig. 3, but data are from 24 Mar 2010.

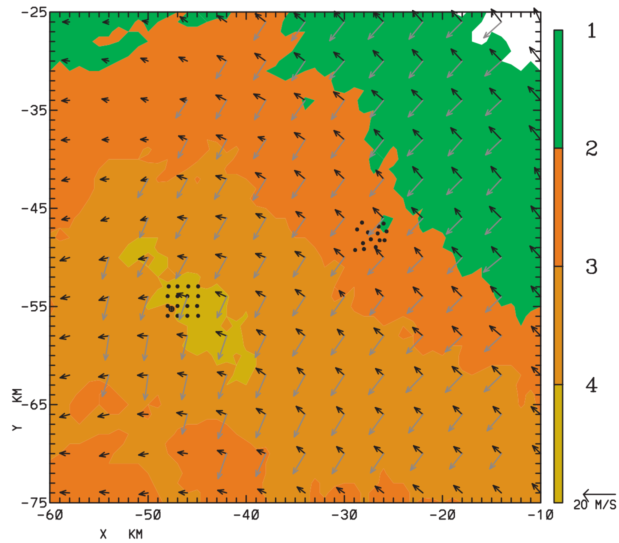

FIG. 16. Trajectory results for 0010–0050 UTC 24 Mar 2010. Plotting conventions are as in Fig. 4 except that upper level (black) is 4.75 km MSL and lower level (gray) is 2.5 km MSL.

In an approximation of the winter-storm observations made by the CSU–CHILL radar, all of the calculations were done using a wavelength of 11 cm, an antenna elevation angle of 3°, and a temperature of −15°C. The hydrometeors were modeled as oblate spheroids. For each particle diameter, T matrices were computed using various bulk density (ice/air fraction) and aspect ratio (vertical/horizontal dimension fraction) values. In general, basic, pristine dendritic particles were assumed to have relatively high bulk densities and relatively small (flat) aspect ratios. In contrast, aggregates were taken to have larger diameters, lower bulk densities, and aspect ratios that approached 1.0 (quasi spherical).

To determine the net radar backscattering characteristics from a population of hydrometeors, a second program that inputs a number of the particle-specific T-matrix files was used. The contributions of these individual T-matrix files were weighted according to a prescribed exponential size distribution. The resultant Mueller matrix provided the basis for calculating the Z_{hh}, K_{DP}, and Z_{DR} values associated with the prescribed ice particle regimes.

The scattering computation results critically depend on the assumptions used to select all of the above-mentioned parameters. Because no detailed observations of snow particle physical characteristics and size distributions are available for the cases considered here, reasonable approximations based on previously published results were used. The hydrometeor observations reported by Lo and Passarelli (1982) were used to guide the specification of the snow particle size distribution. A central element of their study was the collection of Lagrangian-framework in situ data as the sampling aircraft performed a decreasing-altitude spiral maneuver that allowed it to advect with the mean horizontal wind field while descending at a rate approximately equal to the typical mean fall speed of the surrounding snow particles. A primary characteristic of the resultant vertical profiles was the tendency for the hydrometeor size distribution to assume a significantly more flattened (i.e., smaller intercept and reduced slope) configuration when the aircraft descended to altitudes at which active particle aggregation was in progress. Because the CSU–CHILL radar observations indicated that the maximum K_{DP} values were consistently found above the highest reflectivity levels (i.e., presumably associated with the largest particle diameters), the basic size distribution slope and intercept values typical of those observed by Lo and Passarelli prior to the onset of aggregation were used: ($N_0 = 200 \times 10^3$ particles per meter cubed per centimeter and $\lambda = 35$ cm^{-1}).

Figure 18 shows a plot of the basic PSD used in the scattering calculations. The T matrices were computed for each of the 35 marked diameters between 0.2 and 7.0 mm. It was assumed that the particles at the smaller-diameter end of the spectrum were relatively pristine dendritic-type crystals. In accord with this assumption, they were taken to have fairly high bulk densities (0.3–0.5 g cm^{-3}) and distinctly oblate aspect ratios (0.1–0.2). In contrast, the larger-diameter particles were presumed to be aggregates with bulk densities near 0.1 g cm^{-3} and quasi-spherical shapes. (References for the various parameters used in the scattering-model runs are summarized in Table 1.)

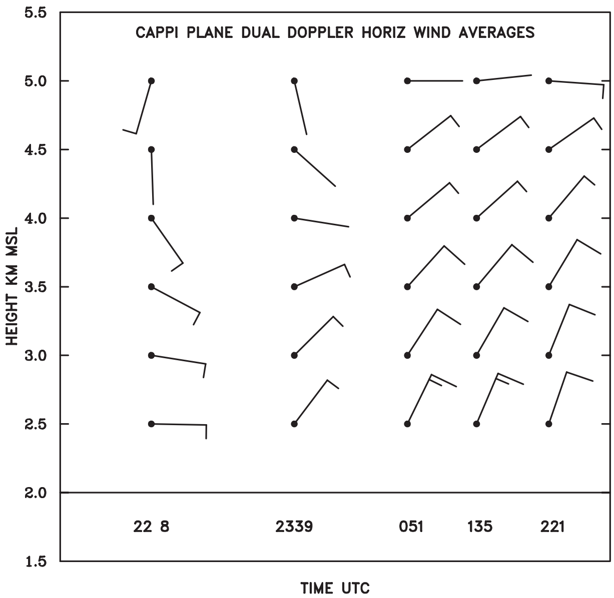

FIG. 17. Time–height plot of horizontal winds based on five dual-Doppler wind field syntheses done using PPI volume-scan data from the CSU–CHILL and KFTG radars on 23–24 Mar 2010. Full barb is 10 m s^{-1}, and half barb is 5 m s^{-1}. The winds are derived from the U and V components averaged over an X domain from −70 to −10 km and a Y domain from −100 to −40 km with respect to the CSU–CHILL radar. (This averaging domain is shown in Fig. 12a.)

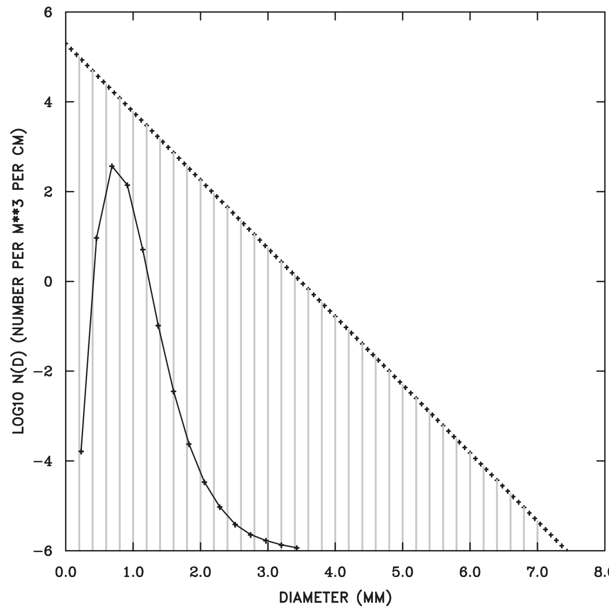

FIG. 18. Example exponential particle size distribution used in the scattering-model calculations. Individual T-matrix calculation diameters are marked by vertical gray lines. The solid curve is the normalized K_{DP} contribution made by dendritic crystals (see text).

The solid curve plotted in the smaller-diameter portion of Fig. 18 shows the normalized K_{DP} contribution made by the pristine crystals in each diameter bin between 0.2 and 5 mm. The ice mass per particle increases with diameter, but the effectiveness of this factor is opposed by the corresponding decrease of concentration with increasing diameter. Under the conditions modeled here, dendritic crystals in the diameter range of 0.8–1.2 mm make the primary contribution to K_{DP}. When the crystal component of the particle population is removed, the remaining low-density, quasi-spherical aggregates generate only negligible K_{DP} magnitudes.

Figure 19 presents the scattering calculation results for various combinations of specifications of slope and intercept values in the PSD. Dendritic characteristics were used for particles of 3-mm diameter and smaller; particles larger than 3 mm were assumed to be aggregates. In Fig. 19a, the dendritic particles were assumed to have aspect ratios of 0.1 and bulk density values given by Heymsfield et al. (2004). These highly oblate shapes and ~0.4 g cm^{-3} bulk densities yield K_{DP} values of ~0.1° km^{-1} or more under most PSD specifications. In Fig. 19b, the ice crystals are made less effective in K_{DP} production by doubling their aspect ratio to 0.2 and decreasing their bulk densities by 25 . It is seen that K_{DP} magnitudes of ~0.1° km^{-1} or more are still possible under many of the modeled slope/intercept combinations. Although not specifically addressed in this model, any riming of the crystals would shift the particle's dielectric properties toward those of solid ice and enhance the polarimetric indications of oriented hydrometeors (Moisseev et al. 2009).

Because the PSD slope parameter defines the relative proportions of the various particle diameters (and their associated axis ratios), the Z_{DR} values shown in Fig. 19 remain constant for a given slope value. As the slope parameter becomes smaller, the PSD flattens, admitting a larger contribution from the larger-sized, more spherically shaped aggregates. This causes the decreasing Z_{DR} trend

TABLE 1. Ice particle characteristics used in scattering-model simulations.

Particle type	Axis ratio	Bulk density (g cm^{-3})	Canting angle std dev (°)
Dendrites	0.1–0.2	0.5–0.3 [Fig. 5 of Heymsfield (1972)]	15 (Bringi and Chandrasekar 2001; p. 475)
Aggregates	0.8–0.9 [Fig. 7 of Brandes et al. (2007)]	~0.15 [Fig. 5 of Heymsfield et al. (2004)]	30 (Kajikawa 1982)

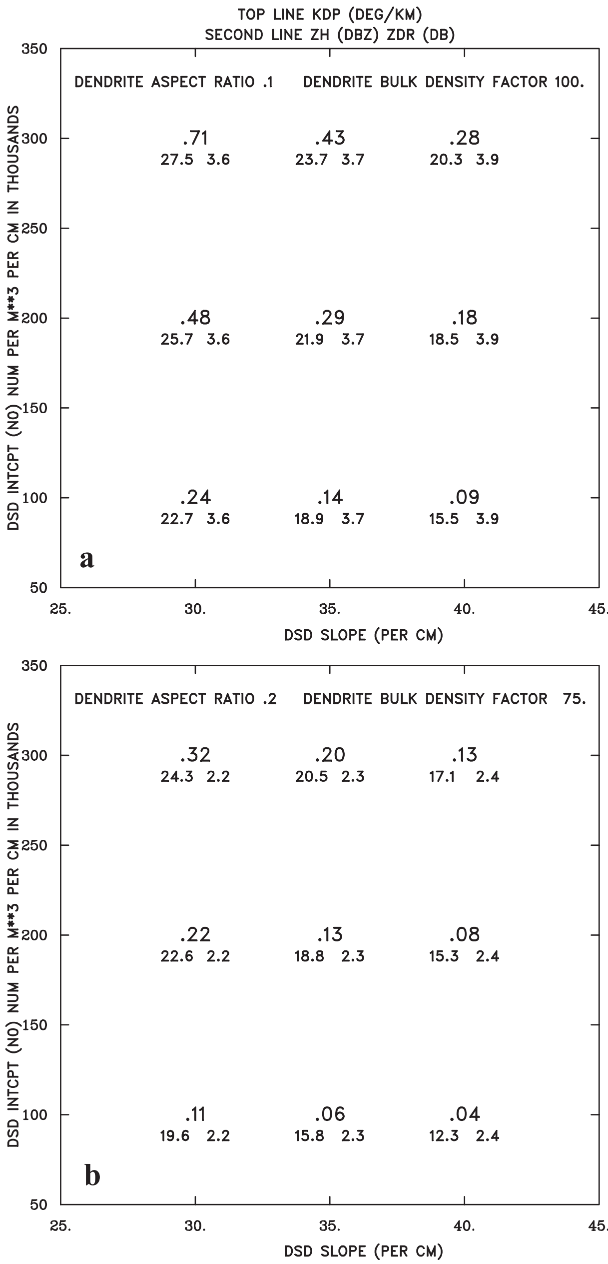

FIG. 19. Scattering-model results under various combinations of dendritic crystal characteristics and PSD specifications. (a) Dendritic-crystal aspect ratio of 0.1, and bulk density given by Heymsfield et al. (2004). (b) Dendritic aspect ratio increased to 0.2, and bulk densities reduced by 25%.

as the slope parameter decreases (Bader et al. 1987; Andric et al. 2010).

The aggregation process has been observed to reduce the slope parameter toward a limiting value of $\sim$10 cm^{-1} and decrease the distribution intercept value as small diameter particles are increasingly ''consumed'' by the growing aggregates (Lo and Passarelli 1982; Braham 1990).

TABLE 2. Scattering-model simulations of PSD with aggregation.

Run	Slope (cm^{-1})	N_0 (cm^{-1} m^{-3})	Dendrite diam (mm)	Z_h (dBZ)	Z_{DR} (dB)	K_{DP} (° km^{-1})
1	12	40×10^3	0.2–3.0	33.8	1.23	0.57
2	12	40×10^3	0.2–0.8	29.6	0.03	0.05

Table 2 summarizes the scattering results when an aggregated PSD is simulated with a slope of 12 cm^{-1} and an N_0 value of 40×10^3. In the first run, in which dendritic particle characteristics are retained in the diameter range of 0.2–3 mm, the flattened PSD slope lowers the Z_{DR} to $\sim$1.2 dB. Despite the partial masking effects of the aggregates, the population of smaller dendritic crystals still generates a large ($\sim$0.6° km^{-1}) K_{DP} magnitude. The K_{DP}'s capability for detecting crystalline (i.e., oblate/relatively high bulk density) particles independently from a coexisting population of aggregates is analogous to the use of K_{DP}-based rain-rate estimators to separate the signal contribution of oblate raindrops from that of quasi-spherical hailstones. In the second model run, a more realistic simulation of aggregation has been done in which the crystal ''consumption'' process has been represented by restricting the dendritic particle characteristics to the diameter range of 0.2–0.8 mm. The resultant minimal Z_{DR} and K_{DP} levels are consistent with the values observed in the vertical profiles at near-surface heights (i.e., Figs. 2, 7, 11, and 14).

5. Particle growth calculations

Because the scattering calculations suggest the importance of relatively high bulk density, oblate ice particles in the general diameter range of 0.8–1.2 mm to the generation of detectable S-band K_{DP} levels, a simple computation of the ice particle growth rate due to vapor deposition was undertaken. The basic growth rate equation given by Pruppacher and Klett [1980, their Eq. (13-71)] that was used was

$$dm/dt = 4\pi C(S - 1)/(A + B),$$

with

$$A = RT/[e(T)DM] \quad \text{and}$$
$$B = [L/(\kappa T)]\{[(LM)/(RT)] - 1\},$$

where C is the capacitance factor for a given ice crystal shape, S is the saturation ratio for ice [$=e_v/e_{si}(T)$], R is the universal gas constant, T is the ambient environmental temperature, $e_{si}(T)$ is saturation vapor pressure over a planar ice surface, D is the diffusivity of water vapor in air, M is the molecular weight of water, L is the latent heat of sublimation, and κ is the thermal conductivity of air.

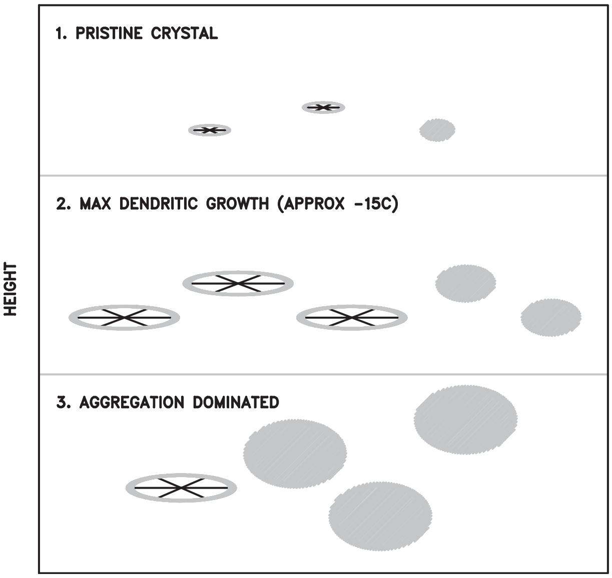

FIG. 20. Conceptual model of the vertical profile of snow particle types in the high-intensity precipitation regions of a northeastern Colorado winter storm. Open symbols with internal radial lines represent generic dendrite-type ice crystals. Diffuse hatched symbols represent aggregated snow particles.

Following the method of Hall and Pruppacher (1976), a ventilation factor adjustment was applied to the basic stationary particle growth rate to account for the augmentation of vapor flux by particle fall speed. The growth calculations were initiated with a 0.2-mm diameter, 0.1-aspect-ratio disk-shaped particle ($C = \pi$/diameter) at an altitude of 6.7 km MSL and a temperature $-28°$C—conditions that approximated the upper levels of the echoes in the RHI scan shown in Fig. 6. The bulk density of the particle was maintained at 0.5 g cm^{-3} throughout the growth process. The growth calculations were done using 100-s time steps. Under the assumed continuously water-saturated growth conditions, the initial particle attained a diameter of 1.7 mm when it reached the $-15°$C temperature level after a descent time of 1.8 h. (The growth rate increased with time; the final 50% of the ending mass value was added during the last ~750 m of the descent.) These simple calculations indicate that continuous vapor deposition growth in suitably deep and moist winter-storm cloud systems is capable of producing ice particles with the physical properties that can generate detectable S-band K_{DP} magnitudes near the $-15°$C temperature level.

Figure 20 is a schematic depiction of the basic features of the winter-storm hydrometeor regimes that have been inferred in this analysis. At the upper levels in lower-temperature and lower-reflectivity portions of winter-season echoes, an environment that is favorable for the existence of pristine ice crystals frequently exists (Ryzhkov and Zrnic 1998). The vertical cross sections presented here did not contain the distinctly positive (several decibels) Z_{DR} values that have been observed in the upper portion of some winter-season echo systems. Because these cross sections intercepted particularly deep echoes associated with high surface snowfall rates, it is suspected that favorable particle growth conditions promoted the formation of enough small aggregates to reduce the observed Z_{DR} magnitudes (Bader et al. 1987). In the central portion of Fig. 20, dendritic particle growth is maximized near the $-15°$C temperature level. The presence of this region of appreciable dendritic particle sizes and concentrations causes local Z_{DR} and K_{DP} enhancements to appear. At the lowest height levels, aggregation transforms much of the snow particle population into low-density, quasi-spherical hydrometeors that generate near-zero levels of Z_{DR} and K_{DP}.

6. Discussion and conclusions

The polarimetric radar observations summarized in this paper have documented the existence of S-band K_{DP} magnitudes of several tenths of a degree per kilometer in the vicinity of the $-15°$C temperature level in regions of active precipitation production in winter storms. The scattering-model results suggest that this K_{DP} pattern appears when significant concentrations of dendritic particles are present in the diameter range of ~0.8–1.2 mm with bulk densities greater than ~0.3 g cm^{-3} and aspect ratios (vertical dimension/horizontal dimension) of ~0.3 or less. The tendency for the positive K_{DP} layer to occur close to the altitude of the $-15°$C isotherm suggests that the vigorous depositional growth of dendritic particles that takes place near this temperature (in a water-saturated environment) is an important factor. The maintenance of this active depositional growth requires that upward air motions provide an adequate water vapor supply to the ice particles. Thus, the observation of positive K_{DP} layers near the $-15°$C level may provide an indication of areas where mesoscale forcing is particularly active, producing rapid ice crystal growth in winter storms. Although snowfall was often observed in the absence of organized positive K_{DP} areas, the more intense surface precipitation rates appear to have some correlation with positive K_{DP} source regions aloft. These results need to be extended to shorter radar wavelengths (with correspondingly greater K_{DP} sensitivity) and to additional climatic regions.

Acknowledgments. The anonymous reviewers are recognized for the several improvements that they suggested to the original manuscript version. Scott Landolt of NCAR's Research Applications Laboratory provided the surface precipitation observations from the Marshall and Denver International Airport observation sites. The scattering model codes were supplied by Dr. Brenda Dolan (CSU Dept. of Atmospheric Science); L. Jay Miller and John Tuttle (both from NCAR) were instrumental in resurrecting the trajectory program. Operations of the CSU–CHILL radar are critically dependent on the technical staff: engineers Dave Brunkow and Jim George along with master technician Robert Bowie. The CSU–CHILL National Radar Facility is funded by NSF Cooperative Agreement ATM 0735110.

REFERENCES

Andric, J., D. Zrnic, J. Straka, and V. Melnikov, 2010: The enhanced Z_{DR} signature in stratiform clouds above melting layer. Preprints, *13th Conf. on Cloud Physics,* Portland, OR, Amer. Meteor. Soc., P2.89. [Available online at http://ams.confex.com/ams/pdfpapers/171308.pdf.]

Bader, M. J., S. A. Clough, and G. P. Cox, 1987: Aircraft and dual polarization observations of hydrometeors in light stratiform precipitation. *Quart. J. Roy. Meteor. Soc.,* **113,** 491–515.

Barber, P., and C. Yeh, 1975: Scattering of electromagnetic waves by arbitrarily shaped dielectric bodies. *Appl. Opt.,* **14,** 2864–2872.

Braham, R. R., 1990: Snow particle spectra in lake effect snows. *J. Appl. Meteor.,* **29,** 200–207.

Brandes, E. A., K. Ikeda, G. Zhang, M. Schoenhuber, and R. M. Rasmussen, 2007: A statistical and physical description of hydrometeor distributions in Colorado snowstorms using a video disdrometer. *J. Appl. Meteor. Climatol.,* **46,** 634–650.

Bringi, V. N., and V. Chandrasekar, 2001: *Polarimetric Doppler Weather Radar*. Cambridge University Press, 636 pp.

Brunkow, D. A., V. N. Bringi, P. C. Kennedy, S. A. Rutledge, V. Chandrasekar, E. A. Mueller, and R. K. Bowie, 2000: A description of the CSU–CHILL National Radar Facility. *J. Atmos. Oceanic Technol.,* **17,** 1596–1608.

Dunn, L. B., 1988: Vertical motion evaluation in a Colorado snowstorm from a synoptician's perspective. *Wea. Forecasting,* **3,** 261–272.

Hall, W. D., and H. R. Pruppacher, 1976: The survival of ice particles falling from cirrus clouds in subsaturated air. *J. Atmos. Sci.,* **33,** 1995–2006.

Heymsfield, A., 1972: Ice crystal terminal velocities. *J. Atmos. Sci.,* **29,** 1348–1357.

——, A. Bansemer, C. Schmitt, C. Twohy, and M. R. Poellot, 2004: Effective ice particle densities derived from aircraft data. *J. Atmos. Sci.,* **61,** 982–1003.

Hogan, R. J., P. R. Field, A. J. Illingworth, R. J. Cotton, and T. W. Choularton, 2002: Properties of embedded convection in warm-frontal mixed-phase cloud from aircraft and polarimetric radar. *Quart. J. Roy. Meteor. Soc.,* **128,** 451–476.

Hubbert, J., and V. N. Bringi, 1995: An iterative filtering technique for the analysis of copolar differential phase and dual-frequency radar measurements. *J. Atmos. Oceanic Technol.,* **12,** 643–648.

Jameson, A. R., 1983: Microphysical interpretation of multiparameter radar measurements in rain. Part II: Estimation of raindrop distribution parameters by combined dual-wavelength and polarization measurements. *J. Atmos. Sci.,* **40,** 1803–1813.

Kajikawa, M., 1982: Observation of the falling motion of early snow flakes Part I. Relationship between free-fall pattern and the number and shape of component snow crystals. *J. Meteor. Soc. Japan,* **60,** 797–803.

Knight, C. A., and K. R. Knupp, 1986: Precipitation growth trajectories in a CCOPE storm. *J. Atmos. Sci.,* **43,** 1057–1073.

Lo, K. H., and R. E. Passarelli Jr., 1982: The growth of snow in winter storms: An airborne observational study. *J. Atmos. Sci.,* **39,** 697–706.

Miller, L. J., C. G. Mohr, and A. J. Weinheimer, 1986: The simple rectification of Cartesian space folded radial velocities from Doppler radar sampling. *J. Atmos. Oceanic Technol.,* **3,** 162–174.

Mohr, C. G., and R. L. Vaughan, 1979: An economical procedure for Cartesian interpolation and display of reflectivity data three-dimensional space. *J. Appl. Meteor.,* **18,** 661–670.

Moisseev, D., E. Saltikov, and M. Leskinen, 2009: Dual-polarization weather radar observations of snow growth processes. Preprints, *34th Conf. on Radar Meteorology,* Williamsburg, VA, Amer. Meteor. Soc., 13B.2. [Available online at http://ams.confex.com/ams/pdfpapers/156123.pdf.]

Poulos, G. S., D. A. Wesley, M. P. Meyers, E. Szoke, and J. S. Snook, 2003: Exceptional mesoscale features of the Great Western Storm of March 16–20, 2003. Preprints, *10th Conf. on Mesoscale Processes,* Portland, OR, Amer. Meteor. Soc., 14.2A/6.6A. [Available online at http://ams.confex.com/ams/pdfpapers/64705.pdf.]

Pruppacher, H. R., and J. D. Klett, 1980: *Microphysics of Clouds and Precipitation*. D. Reidel, 714 pp.

Rasmussen, R. M., A. Crook, and C. Kessinger, 1993: Snow-band formation and evolution during the 15 November 1987 aircraft accident at Denver airport. *Wea. Forecasting,* **8,** 453–480.

Ryzhkov, A. V., and D. S. Zrnic, 1998: Discrimination between rain and snow with polarimetric radar. *J. Appl. Meteor.,* **37,** 1228–1240.

——, ——, and B. A. Gordon, 1998: Polarimetric method for ice water content determination. *J. Appl. Meteor.,* **37,** 125–134.

Trapp, J. R., D. M. Schultz, A. V. Ryzhkov, and R. L. Holle, 2001: Multiscale structure and evolution of an Oklahoma winter precipitation event. *Mon. Wea. Rev.,* **129,** 486–501.

Wang, Y., and V. Chandrasekar, 2009: Algorithm for the estimation of specific differential phase. *J. Atmos. Oceanic Technol.,* **26,** 61–78.

Waterman, P. C., 1971: Symmetry, unitarity and geometry in electromagnetic scattering. *Phys. Rev.,* **3,** 825–839.